Advanced Robotics

ISSN: 0169-1864 (Print) 1568-5535 (Online) Journal homepage: https://www.tandfonline.com/loi/tadr20

Robust Adaptive Stabilization of Skid Steer Wheeled Mobile Robots Considering Slipping Effects

E. Mohammadpour & M. Naraghi

To cite this article: E. Mohammadpour & M. Naraghi (2011) Robust Adaptive Stabilization of Skid Steer Wheeled Mobile Robots Considering Slipping Effects, Advanced Robotics, 25:1-2, 205-227, DOI: 10.1163/016918610X538552

To link to this article: https://doi.org/10.1163/016918610X538552

Published online: 02 Apr 2012.

VSP

Advanced Robotics 25 (2011) 205–227

ADVANCED ROBOTICS
brill.nl/ar

Full paper

Robust Adaptive Stabilization of Skid Steer Wheeled Mobile Robots Considering Slipping Effects

E. Mohammadpour and M. Naraghi *

Department of Mechanical Engineering, AmirKabir University of Technology, 424 Hafez Avenue, PO Box 15875-4413, Tehran, Iran

Received 8 December 2009; accepted 8 February 2010

Abstract

This paper represents the posture stabilization of a skid steer wheeled mobile robot (SSWMR). Although in mobile robots lateral skidding of the wheels occurs when turning at high speed, wheels of a SSWMR laterally skid in every rotational maneuver even at low speeds. Also, longitudinal slipping for wheeled mobile robots with pneumatic tires is inevitable due to tire deformation. In order to compensate for the effects of tire slippage and parameter uncertainties, an adaptive torque controller is developed based on a tunable dynamic oscillator. The globally uniformly ultimately bounded stability of the system to an arbitrarily small neighborhood of the origin is proved. The internal dynamics stability of the system is guaranteed employing a supervisory fuzzy logic-based controller. To demonstrate the performance of the proposed controller, modeling of a SSWMR was implemented through automatic dynamic analysis of mechanical systems (ADAMS).

Keywords

Posture stabilization, skid steer, robust adaptive control, longitudinal slipping, ADAMS

1. Introduction

Wheeled mobile robots are widely used in a variety of fields of industrial applications. Numerous studies have been presented for the control of wheeled mobile robots based on the hypothesis of non-skidding kinematic constraints. However, in real robots, especially when turning at high speed, the cornering force of the robot tires might not be large enough to prevent skidding along the lateral direction of the wheels and, thus, the non-holonomic constraint will not be satisfied. In addition, longitudinal slipping for wheeled mobile robots with pneumatic tires is inevitable due to tire deformation.

* To whom correspondence should be addressed. E-mail: naraghi@aut.ac.ir

 DOI:10.1163/016918610X538552

Recently, many researchers have considered the effects of skidding and slipping of robot wheels for trajectory tracking and path following problems. Leroquais and d'Andrea-Novel [1] and Motte and Campion [2] studied the trajectory tracking of wheeled mobile robots at the dynamic level based on the exact knowledge of the system parameters. Urakubo *et al.* [3] proposed a Lyapunov-based kinematic controller for two-wheeled mobile robots considering skidding of the robot wheels. Zhang *et al.* [4] presented a robust controller based on the sliding mode technique for trajectory tracking of a differentially steered mobile robot considering elastic tire effects. Wang *et al.* [5] developed a robust adaptive controller for the trajectory tracking of wheeled mobile robots based on the backstepping technique. Low and Wang [6, 7] developed a GPS-based kinematic controller for car-like wheeled mobile robots taking into account the skidding and slipping effects. Also, they considered the modeling and analysis of skidding and slipping in different configurations of wheeled mobile robots [8]. Martins *et al.* [9] presented an adaptive controller for trajectory tracking of a unicycle-like mobile robot including motor dynamics. Also, Ploeg *et al.* [10] proposed a nonlinear controller for trajectory tracking of an overactuated multi-cycle robot considering the effects of elastic tires and slipping of the wheels.

In a skid steer wheeled mobile robot (SSWMR), steering is accomplished by creating a differential velocity between the inner and outer wheels leading to lateral skidding of the wheels in every rotational maneuver even for low speeds. Some of researchers considered the trajectory tracking problem for these kinds of mobile robots. Caracciolo *et al.* [11] presented a robust torque controller for a SSWMR using the feedback linearization technique. Maalouf *et al.* [12] proposed a higher-level fuzzy logic-based control for path tracking of a SSWMR. Yi *et al.* [13] considered the effects of longitudinal slipping on a SSWMR. They proposed an adaptive controller for trajectory tracking of the robot. However, in these works, the longitudinal component of the instantaneous center of rotation (ICR) is assumed to be constant during robot motion, which cannot be enforced in practice. Observations show that at low speeds, the longitudinal component of the ICR is approximately equal to zero ($x_{\mathrm{icr}} \approx 0$), but for high-speed rotational maneuvers, it becomes large and may move out of the robot wheelbase, causing loss of motion stability.

The other problem that has received the great attention of many researchers in recent years is the posture stabilization problem. Due to Brockett's theorem [14], non-holonomic systems with restricted mobility cannot be stabilized to a desired posture *via* smooth state feedback [15]. Although there are various approaches for the posture stabilization of wheeled mobile robots (e.g., Refs [16–20]), only few works have considered the effect of skidding and slipping of the robot wheels in posture stabilization of wheeled mobile robots. Corradini *et al.* [21] proposed a discrete kinematic stabilizing controller for posture stabilization of wheeled mobile robots *via* quasi-sliding modes. They designed controllers based on the assumption that the non-skidding constraint was violated. Dixon *et al.* [22] developed a kinematic controller based on the dynamic oscillator that is applicable for both the

tracking and stabilization problems. They considered skidding and slipping of robot wheels as a kinematic disturbance making the non-holonomic constraint of pure rolling and non-skidding of robot wheels violated.

Recently, posture stabilization of SSWMRs was studied by Kozlowski and Pazderski [23]. They presented a control law based on Dixon's tunable dynamic oscillator [24] that solves a unified tracking and regulation problem. Although they developed a posture stabilizing controller for SSWMRs, x_{icr} was assumed to be a nonzero constant. They continued their works on SSWMRs and developed kinematic controllers for the posture stabilization problem in which the non-practical constraint of constant ICR has been eliminated [25, 26]. In fact, they designed a controller in such a manner that the ICR is kept in the robot wheelbase during the motion. However, in their kinematic-based controller, longitudinal slipping of the robot wheels was not considered. Also, it was assumed that desired wheel velocities are readily available by ignoring robots dynamics. However, it is more realistic to formulate the system at the dynamic level where the torque and force are taken as the control inputs. In addition, it is almost impossible to obtain exact values of parameters of a real mobile robot and then the effects of model uncertainties of dynamical systems should be compensated for.

In this paper, a robust adaptive stabilization control of SSWMRs considering tire slippage and parametric uncertainties is presented. To provide more realistic conditions, modeling of a SSWMR was implemented through ADAMS (Automatic Dynamic Analysis of Mechanical Systems). The effects of longitudinal slipping and wheel dynamics are considered and globally uniformly ultimately bounded (GUUB) stability of the system to an arbitrarily small neighborhood of the origin is proved. Also, a supervisory fuzzy logic-based controller is designed to keep the ICR in the robot wheelbase during the motion and the stability of internal dynamics is established. This paper is organized as follows. In Section 2, modeling of a SSWMR is presented. Controller design is performed in Section 3. Simulation results are shown in Section 4. Section 5 includes the conclusions of the study.

2. Modeling

In this section, the modeling of a four-wheeled SSWMR is obtained to use in controller design. The kinematic and dynamic equations of motion are derived mathematically, and then transformed to an appropriate form to facilitate the subsequent control synthesis and stability analysis.

2.1. Kinematic and Dynamic Modeling

The kinematic model of non-holonomic 'unicycle' mobile robots is given by:

$$\dot{\mathbf{q}} = \mathbf{S}(\mathbf{q})\mathbf{v}, \tag{1}$$

where $\mathbf{q} = [x_c \;\; y_c \;\; \theta]^{\mathrm{T}}$ in which x_c and y_c are the positions of the robot center of mass (COM) along with the X and Y global coordinate frames, and θ is the orien-

tation of the robot. $\mathbf{v} = [v_x \ \ \Omega]^{\mathrm{T}}$ denotes the vector of linear and angular velocity of the robot and $\mathbf{S}(\mathbf{q})$ is defined as:

$$\mathbf{S}(\mathbf{q}) = \begin{bmatrix} \cos\theta & 0 \\ \sin\theta & 0 \\ 0 & 1 \end{bmatrix}. \tag{2}$$

The following relation, which is called the pure rolling and non-skidding kinematic constraint of the robot, is held on (1):

$$\dot{x}_{\mathrm{c}} \sin\theta - \dot{y}_{\mathrm{c}} \cos\theta = 0. \tag{3}$$

This constraint is violated on the SSWMR in every rotational maneuver due to the lateral skidding of the wheels. Thus, kinematic modeling of a four-wheeled SSWMR can be expressed as:

$$\dot{\mathbf{q}} = \mathbf{S}(\mathbf{q})\mathbf{v} + \mathbf{A}(\mathbf{q})v_y, \tag{4}$$

where:

$$\mathbf{A}(\mathbf{q}) = [-\sin\theta \quad \cos\theta \quad 0]^{\mathrm{T}}, \tag{5}$$

is in the null space of the columns of $\mathbf{S}(\mathbf{q})$ and v_y is the lateral velocity of the robot COM.

A free-body diagram of a four-wheeled SSWMR is depicted in Fig. 1. The summation of the external forces and moments in the body-centered reference frame yields to the following equations:

$$\begin{aligned} m(\dot{v}_x - v_y\Omega) &= F_{x\mathrm{l}} + F_{x\mathrm{r}} \\ m(\dot{v}_y + v_x\Omega) &= F_{y\mathrm{f}} + F_{y\mathrm{b}} \\ I_z\dot{\Omega} &= t(F_{x\mathrm{r}} - F_{x\mathrm{l}}) + aF_{y\mathrm{f}} - bF_{y\mathrm{b}} \\ I_{\mathrm{w}}\dot{\omega}_{\mathrm{l}} &= n\tau_{\mathrm{l}} - rF_{x\mathrm{l}} \\ I_{\mathrm{w}}\dot{\omega}_{\mathrm{r}} &= n\tau_{\mathrm{r}} - rF_{x\mathrm{r}}, \end{aligned} \tag{6}$$

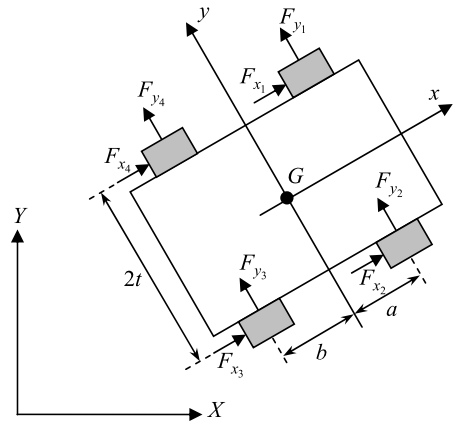

Figure 1. Free-body diagram of the robot.

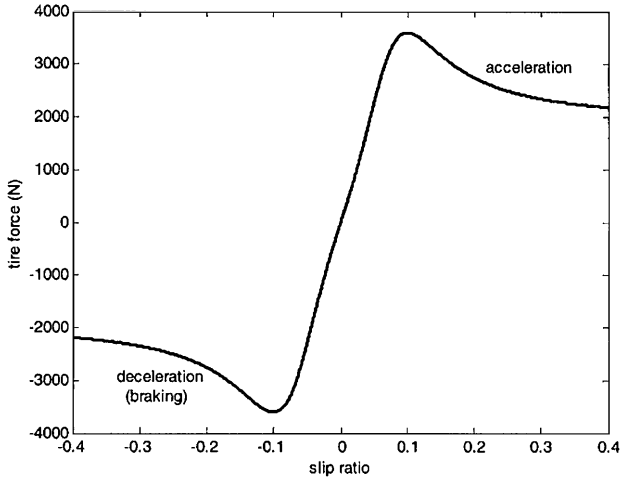

Figure 2. Longitudinal tire force as a function of slip ratio.

where m is the robot mass, I_z is the moment of inertia of robot, I_{w} is the moment of inertia of the wheels, r is the wheel radius, n is the gear ratio, $2t$ is the length of the axis between the wheels, a and b are the distances between the COM and the front and rear axles, respectively, and ω_{l} and ω_{r} are the angular velocity of the left and right wheels of the robot, respectively. τ_{l} and τ_{r} are the left and right motor torques, respectively. $F_{x\mathrm{l}}$ and $F_{x\mathrm{r}}$ are the total longitudinal forces of the left and right wheels, respectively, and F_{yf} and F_{yb} are the total lateral friction forces of the front and rear wheels, respectively.

If the constraint of pure rolling holds, we can obtain the longitudinal velocity of the left and right wheels by $v_{x\mathrm{l}} = r\omega_{\mathrm{l}}$ and $v_{x\mathrm{r}} = r\omega_{\mathrm{r}}$. Generally, this constraint does not hold during the motion. For example, when a robot moves on a slippery surface, the robot wheels may slip even for low speeds. Also, the robot tires usually are not rigid and deformation of pneumatic tires yields to the slipping of robot wheels. When an external torque is applied to a pneumatic tire, longitudinal tire force and slip ratio (normalized slip) are related as shown in Fig. 2. Based on Fig. 2, a tractive longitudinal force exists whenever the slip is non-zero. This means that in the case of pneumatic tires, the pure rolling constraint holds only when the robot is at rest or in the free rolling state.

Now, in order to compare the results, we consider two cases: in 'Case A' wheel dynamics and tire slippage are taken into account, and in 'Case B' those are not considered in modeling of the robot.

2.1.1. Case A

When a robot with pneumatic tires moves on a ground surface and an external torque is applied to the robot wheels, there exists a percentage of wheel slippage between the tires and the ground surface. However, modeling of longitudinal tire force *versus* the slip ratio is not usually performed in control objectives due to its

complexity. Thus, in a similar approach to Ref. [4], slip speeds are assumed to be model uncertainties such that:

$$v_{x\mathrm{l}} = r\omega_{\mathrm{l}} - v_{\mathrm{l}}^{\mathrm{s}}, \qquad v_{x\mathrm{r}} = r\omega_{\mathrm{r}} - v_{\mathrm{r}}^{\mathrm{s}} \tag{7}$$

in which $v_{\mathrm{l}}^{\mathrm{s}}$ and $v_{\mathrm{r}}^{\mathrm{s}}$ are the longitudinal slip speeds of the left and right wheels, respectively.

Remark 1. It has been emphasized that both the lateral skidding and longitudinal slipping of the robot wheels are considered in (4) and (7), respectively.

Using (7), linear and angular velocities of the robot can be expressed as:

$$\begin{aligned} v_x &= \frac{1}{2}(v_{x\mathrm{r}} + v_{x\mathrm{l}}) = \frac{r}{2}(\omega_{\mathrm{r}} + \omega_{\mathrm{l}}) - \frac{1}{2}(v_{\mathrm{r}}^{\mathrm{s}} + v_{\mathrm{l}}^{\mathrm{s}}) \\ \Omega &= \frac{1}{2t}(v_{x\mathrm{r}} - v_{x\mathrm{l}}) = \frac{r}{2t}(\omega_{\mathrm{r}} - \omega_{\mathrm{l}}) - \frac{1}{2t}(v_{\mathrm{r}}^{\mathrm{s}} + v_{\mathrm{l}}^{\mathrm{s}}). \end{aligned} \tag{8}$$

Differentiating (8) and using (6) to eliminate $F_{x\mathrm{l}}$ and $F_{x\mathrm{r}}$ yields the following equations:

$$\begin{aligned} m_{\mathrm{e}}\dot{v}_x &= 2nr\tau_1 + mr^2\Omega v_y - \delta_1 \\ I_{\mathrm{e}}\dot{\Omega} &= 2tnr\tau_2 + r^2(aF_{y\mathrm{f}} - bF_{y\mathrm{b}}) - \delta_2, \end{aligned} \tag{9}$$

where:

$$\begin{aligned} m_{\mathrm{e}} &= 2I_{\mathrm{w}} + mr^2, & I_{\mathrm{e}} &= 2t^2 I_{\mathrm{w}} + r^2 I_{\mathrm{z}} \\ \delta_1 &= I_{\mathrm{w}}(\dot{v}_{\mathrm{r}}^{\mathrm{s}} + \dot{v}_{\mathrm{l}}^{\mathrm{s}}), & \delta_2 &= tI_{\mathrm{w}}(\dot{v}_{\mathrm{r}}^{\mathrm{s}} - \dot{v}_{\mathrm{l}}^{\mathrm{s}}) \\ \tau_1 &= \frac{\tau_{\mathrm{r}} + \tau_{\mathrm{l}}}{2}, & \tau_2 &= \frac{\tau_{\mathrm{r}} - \tau_{\mathrm{l}}}{2}. \end{aligned} \tag{10}$$

Thus, the dynamic model can be expressed in matrix form as:

$$\begin{aligned} \mathbf{M}\dot{\mathbf{v}} + \mathbf{E}(\mathbf{v}, v_y) + \boldsymbol{\tau}_\delta &= \mathbf{B}\boldsymbol{\tau} \\ \dot{v}_y &= \frac{1}{m}(F_{y\mathrm{f}} + F_{y\mathrm{b}}) - v_x\Omega, \end{aligned} \tag{11}$$

where:

$$\begin{aligned} \mathbf{M} &= \begin{bmatrix} m_{\mathrm{e}} & 0 \\ 0 & I_{\mathrm{e}} \end{bmatrix}, & \mathbf{B} &= 2nr \begin{bmatrix} 1 & 0 \\ 0 & t \end{bmatrix} \\ \mathbf{E}(\mathbf{v}, v_y) &= r^2 \begin{bmatrix} -m\Omega v_y \\ bF_{y\mathrm{b}} - aF_{y\mathrm{f}} \end{bmatrix}, & \boldsymbol{\tau}_\delta &= \begin{bmatrix} \delta_1 \\ \delta_2 \end{bmatrix}. \end{aligned} \tag{12}$$

Experimental results show that the lateral force of a tire is proportional to the 'slip angle' for small slip angles. The slip angle of a tire is defined as the angle between the orientation of the tire and orientation of the velocity vector of the wheel. Generally, the slip angle of a wheel is [27]:

$$\alpha = \delta - \theta_{\mathrm{v}}, \tag{13}$$

where θ_v is the angle that the velocity vector makes with the longitudinal axis of the vehicle and δ is the wheel steering angle. In SSWMRs $\delta = 0$ and then slip angle can be calculated by

$$\alpha_i = -\tan^{-1}\left(\frac{\dot{y}_i}{\dot{x}_i}\right), \quad i = 1, \ldots, 4, \tag{14}$$

where $\dot{x}_i$ and $\dot{y}_i$ are the longitudinal and lateral velocities of the wheels COM. For large slip angles, a more sophisticated model is required. However, in controller design it is not necessary to use such a complicated model. Therefore, the following smooth function is proposed based on the idea developed in Ref. [28] for the modeling of tire forces:

$$\begin{aligned} F_{yf} &= \frac{b}{2L}\mu mg[\text{sign}(\alpha_1)(1-\exp(-C_\alpha|\alpha_1|)) \\ &\qquad + \text{sign}(\alpha_2)(1-\exp(-C_\alpha|\alpha_2|))] \\ F_{yb} &= \frac{a}{2L}\mu mg[\text{sign}(\alpha_3)(1-\exp(-C_\alpha|\alpha_3|)) \\ &\qquad + \text{sign}(\alpha_4)(1-\exp(-C_\alpha|\alpha_4|))], \end{aligned} \tag{15}$$

where C_α is a positive constant and $L = a + b$. It has been noted that for small slip angles $F_{yf} = \frac{b}{2L}\mu mgC_\alpha(\alpha_1 + \alpha_2)$ and $F_{yb} = \frac{a}{2L}\mu mgC_\alpha(\alpha_3 + \alpha_4)$. Hence, $\frac{b}{2L}\mu mgC_\alpha$ and $\frac{b}{2L}\mu mgC_\alpha$ are the lateral stiffness of the front and rear wheels tire, respectively.

2.1.2. Case B

In this case, wheel dynamics and tire slippage are neglected. Therefore, in order to obtain the equation of motion it is enough to assume that $I_w = 0$ and $v_r^s = v_l^s \equiv 0$. Therefore, supposing $m_e = mr^2$, $I_e = r^2 I_z$ and $\boldsymbol{\tau}_\delta = [0\ \ 0]^T$, (11) and (12) are held in this case too. Also, in this case, we assume that the lateral forces are simplified by Coulomb friction as:

$$\begin{aligned} F_{yf} &= -\frac{b}{2L}\mu mg\,\text{sign}(\dot{y}_f)(1-\exp(-k_v|\dot{y}_f|)) \\ F_{yb} &= -\frac{a}{2L}\mu mg\,\text{sign}(\dot{y}_b)(1-\exp(-k_v|\dot{y}_b|)), \end{aligned} \tag{16}$$

where μ is the lateral friction coefficient, k_v is a positive constant, and $\dot{y}_f$ and $\dot{y}_b$ are the lateral velocities of the front and rear wheels, respectively.

2.2. Model Transformation

In this section, kinematic and dynamic equations of motion are transformed to an appropriate form suitable for controller design. Without lack of generality, the final desired posture of the robot is assumed to be $\mathbf{q} = [0\ \ 0\ \ 0]^T$. In order to rewrite the kinematic model given in (1) in a form that facilitates the subsequent control synthesis and stability analysis, we use a global invertible transformation as [24]:

$$\mathbf{x} = \mathbf{P}(\boldsymbol{\theta})\mathbf{q}, \tag{17}$$

where $\mathbf{x} = \begin{bmatrix}\mathbf{x}^{*\mathrm{T}} & x_3\end{bmatrix}^{\mathrm{T}} = [x_1 \;\; x_2 \;\; x_3]^{\mathrm{T}}$ and:

$$\mathbf{P}(\boldsymbol{\theta}) = \begin{bmatrix} 0 & 0 & 1 \\ \cos\theta & \sin\theta & 0 \\ -\theta\cos\theta + 2\sin\theta & -\theta\sin\theta - 2\cos\theta & 0 \end{bmatrix}. \tag{18}$$

After taking the time derivative of (17) and using (1) and (2), we can rewrite the stabilizing error dynamics in a form that is similar to Brockett's non-holonomic integrator [14] as:

$$\begin{aligned} \dot{\mathbf{x}}^* &= \mathbf{u} \\ \dot{x}_3 &= \mathbf{x}^{*\mathrm{T}}\mathbf{J}\mathbf{u} + \rho, \end{aligned} \tag{19}$$

where $\rho = -2v_y$ is assumed to be bounded as $|\rho| \leqslant \rho_0$ and $\mathbf{J} \in \Re^{2\times 2}$ is a skew symmetric matrix defined by:

$$\mathbf{J} = \begin{bmatrix} 0 & -1 \\ 1 & 0 \end{bmatrix}, \tag{20}$$

and auxiliary input vector $\mathbf{u}$ is related to $\mathbf{v}$ as:

$$\mathbf{u} = \mathbf{T}^{-1}\mathbf{v} \rightarrow \mathbf{v} = \mathbf{T}\mathbf{u}, \tag{21}$$

where:

$$\mathbf{T} = \begin{bmatrix} x_{\mathrm{c}}\sin\theta - y_{\mathrm{c}}\cos\theta & 1 \\ 1 & 0 \end{bmatrix}. \tag{22}$$

Multiplying the first equation of (11) by $\mathbf{T}^{\mathrm{T}}$ and applying (21) yields the following transformed dynamic model:

$$\overline{\mathbf{M}}\dot{\mathbf{u}} + \overline{\mathbf{V}}_{\mathrm{m}}\mathbf{u} + \overline{\mathbf{N}} + \bar{\boldsymbol{\tau}}_{\delta} = \overline{\mathbf{B}}\boldsymbol{\tau}, \tag{23}$$

where:

$$\begin{aligned} &\overline{\mathbf{M}} = \mathbf{T}^{\mathrm{T}}\mathbf{M}\mathbf{T}, \qquad \overline{\mathbf{V}}_{\mathrm{m}} = \mathbf{T}^{\mathrm{T}}\mathbf{M}\dot{\mathbf{T}}, \qquad \overline{\mathbf{N}} = \mathbf{T}^{\mathrm{T}}\mathbf{E}(\mathbf{T}\mathbf{u}) \\ &\bar{\boldsymbol{\tau}}_{\delta} = \mathbf{T}^{\mathrm{T}}\boldsymbol{\tau}_{\delta}, \qquad \overline{\mathbf{B}} = \mathbf{T}^{\mathrm{T}}\mathbf{B}. \end{aligned} \tag{24}$$

Note that (23) is a common form of dynamic equations of motion for a wide range of robotic applications that is appropriate for control objectives. Several properties associated with the transformed dynamic model will be employed during the subsequent control development and stability analysis of the controllers [29].

Property 1. The transformed inertia matrix $\overline{\mathbf{M}}$ is symmetric, positive definite and satisfies the following inequalities:

$$\forall \boldsymbol{\zeta} \in \Re^2 \quad m_1\|\boldsymbol{\zeta}\|^2 \leqslant \boldsymbol{\zeta}^{\mathrm{T}}\overline{\mathbf{M}}\boldsymbol{\zeta} \leqslant m_2(\mathbf{x})\|\boldsymbol{\zeta}\|^2, \tag{25}$$

where m_1 is a known positive constant and $m_2(\mathbf{x})$ is a known, positive bounding function that is assumed to be bounded provided that its arguments are bounded

(m_1 and $m_2(\mathbf{x})$ denote the minimum and maximum eigenvalues of $\overline{\mathbf{M}}$, respectively). Also it can be proved that the inverse of $\overline{\mathbf{M}}$ satisfies:

$$\forall \boldsymbol{\zeta} \in \Re^2 \quad \frac{1}{m_2(\mathbf{x})}\|\boldsymbol{\zeta}\|^2 \leqslant \boldsymbol{\zeta}^{\mathrm{T}}\overline{\mathbf{M}}^{-1}\boldsymbol{\zeta} \leqslant \frac{1}{m_1}\|\boldsymbol{\zeta}\|^2. \tag{26}$$

Property 2. The matrix $\dot{\overline{\mathbf{M}}} - 2\bar{\mathbf{V}}_{\mathrm{m}}$ is skew symmetric.

Property 3. The robot dynamics (23) without unmodeled dynamics can be linearly parameterized as:

$$\overline{\mathbf{M}}\dot{\mathbf{u}} + \overline{\mathbf{V}}_{\mathrm{m}}\mathbf{u} + \overline{\mathbf{N}} = \boldsymbol{\Upsilon}\vartheta, \tag{27}$$

where $\vartheta \in \Re^p$ contains the constant mechanical parameters of the system and $\boldsymbol{\Upsilon} \in \Re^{2\times p}$ denotes a known regression matrix.

3. Control Development

In this section, the kinematic control law for the stabilization problem is developed based on the dynamic oscillator [24]. Afterwards, a robust adaptive controller will be designed by using the standard backstepping technique to suppress undesirable effects of tire slippage and parametric uncertainties associated with the dynamic model (i.e., mass, inertia and friction coefficients). Finally, a higher-level supervisory fuzzy controller is developed to establish the lateral motion stability.

Problem definition. Find a bounded control input vector ($\mathbf{v}$ or $\boldsymbol{\tau}$), such that for any initial posture $\mathbf{q}(0)$, $\lim_{t\to\infty}\|\mathbf{q}(t)\| < \varepsilon$, where $\varepsilon > 0$ is an assumed error envelope that can be made arbitrarily small.

3.1. Kinematic Control Law

The new state vector is defined by:

$$\mathbf{z} = [\,\mathbf{z}^{*\mathrm{T}} \quad z_3\,]^{\mathrm{T}} = [\,\mathbf{x}^{*\mathrm{T}} - \mathbf{x}_{\mathrm{d}}^{*\mathrm{T}} \quad x_3 + \mathbf{x}_{\mathrm{d}}^{*\mathrm{T}}\mathbf{J}\mathbf{x}^*\,]^{\mathrm{T}}, \tag{28}$$

in which $\mathbf{x}_{\mathrm{d}}^*$ is an auxiliary signal, originated by a tunable oscillator, according to the following equation:

$$\mathbf{x}_{\mathrm{d}}^* = \boldsymbol{\Psi}\boldsymbol{\xi} \tag{29}$$

where $\boldsymbol{\Psi} = \mathrm{diag}\{\psi_1, \psi_2\}$ is a positive definite matrix where ψ_1 and ψ_2 are assumed to be:

$$\psi_i = a_i \exp(-\alpha_i t) + \varepsilon_i, \quad i = 1, 2, \tag{30}$$

in which a_i, α_i and ε_i are positive constants. Also, $\boldsymbol{\xi}$ is the solution of:

$$\dot{\boldsymbol{\xi}} = u_{\mathrm{w}}\mathbf{J}\boldsymbol{\xi}, \quad \|\boldsymbol{\xi}(0)\| = 1, \tag{31}$$

where u_w represents the instantaneous frequency of $\boldsymbol{\xi}$. It can be easily proved that:

$$\frac{d}{dt}(\boldsymbol{\xi}^T\boldsymbol{\xi}) = 0 \quad \Rightarrow \quad \forall t \geqslant 0 \quad \|\boldsymbol{\xi}(t)\| = \|\boldsymbol{\xi}(0)\| = 1. \tag{32}$$

After taking the time derivative of (28), the following equation will be obtained:

$$\begin{bmatrix} \dot{\mathbf{z}}^* \\ \dot{z}_3 \end{bmatrix} = \begin{bmatrix} \mathbf{u} - \dot{\mathbf{x}}_d^* \\ (\mathbf{z}^{*T} + 2\mathbf{x}_d^{*T})\mathbf{J}\mathbf{u} + \dot{\mathbf{x}}_d^{*T}\mathbf{J}(\mathbf{z}^* + \mathbf{x}_d^*) + \rho \end{bmatrix}. \tag{33}$$

Proposition 1. *The control law represented by:*

$$\mathbf{u} = \dot{\mathbf{x}}_d^* - k_1\mathbf{z}^*, \tag{34}$$

and the instantaneous frequency:

$$u_w = \frac{1}{\psi_1\psi_2}\{k_2 z_3 + \boldsymbol{\xi}^T\boldsymbol{\Psi}^T\mathbf{J}\dot{\boldsymbol{\Psi}}\boldsymbol{\xi} + 2k_1\mathbf{z}^{*T}\mathbf{J}\mathbf{x}_d^* + h_z\}, \tag{35}$$

where $h_z = \frac{\rho_0^2}{\rho_0|z_3| + \varepsilon_z} z_3$, *ensures GUUB tracking and regulation of* (33) *in a sense that:*

$$\mathbf{z}^*(t) = \mathbf{z}^*(0)\exp(-k_1 t) \tag{36a}$$

$$|z_3(t)| \leqslant \sqrt{z_3^2(t)\exp(-2k_2 t) + \frac{\varepsilon_z}{k_2}(1 - \exp(-2k_2 t))}, \tag{36b}$$

where k_1, k_2 *and* ε_z *are positive constants.*

Proof. Exploiting (33), (34) and (35), the closed-loop error dynamics is given by:

$$\dot{\mathbf{z}}^* = -k_1\mathbf{z}^* \tag{37a}$$

$$\dot{z}_3 = -k_2 z_3 + (\rho - h_z), \tag{37b}$$

(37a) can be simply proved (36a). Now, consider the radially unbounded Lyapunov function

$$V_1 = \frac{1}{2}z_3^2. \tag{38}$$

After taking the time derivative of (38) and using (37b), the following expression will be obtained:

$$\dot{V}_1 = -k_2 z_3^2 + z_3(\rho - h_z) \leqslant -k_2 z_3^2 + \frac{\rho_0|z_3|}{\rho_0|z_3| + \varepsilon_z}\varepsilon_z \leqslant -2k_2 V_1 + \varepsilon_z. \tag{39}$$

Lemma 1 of Appendix and (39) can be invoked to prove (36b). QED.

Remark 2. Based on (36) it is straightforward that $\mathbf{z}(t) \in \ell_\infty$. Using (29) and observing the fact that $\boldsymbol{\Psi}(t)$, $\boldsymbol{\xi}(t) \in \ell_\infty$, it can be concluded that $\mathbf{x}_d^*(t) \in \ell_\infty$. Thus, (28) can be employed to conclude that $\mathbf{x}(t) \in \ell_\infty$. Based on (30), it is obvious that $\dot{\boldsymbol{\Psi}}(t) \in \ell_\infty$. Utilizing (35) concluded that $u_w(t) \in \ell_\infty$. Thus, $\dot{\mathbf{x}}_d^* \in \ell_\infty$ and, therefore, from (34) it can be concluded that $\mathbf{u}(t) \in \ell_\infty$.

Remark 3. Using (36), it can be simply observed that:

$$\begin{aligned} &\lim_{t\to\infty} \|\mathbf{x}^*\| \leqslant \varepsilon_{\mathrm{m}} = e_1 \\ &\lim_{t\to\infty} |x_3| \leqslant \sqrt{\frac{\varepsilon_z}{k_2}} + \varepsilon_{\mathrm{m}}^2 = e_2, \end{aligned} \tag{40}$$

where $\varepsilon_{\mathrm{m}} = \sqrt{\varepsilon_1^2 + \varepsilon_2^2}$. Therefore:

$$\begin{aligned} &\lim_{t\to\infty} |x_{\mathrm{c}}|, |y_{\mathrm{c}}| \leqslant \frac{1}{2}\big(e_1\sqrt{e_1^2+4} + e_2\big) \\ &\lim_{t\to\infty} |\theta| \leqslant e_1. \end{aligned} \tag{41}$$

3.2. Robust Adaptive Control Law

In this section, an adaptive backstepping control technique, which is a standard advanced technique of robust control, is employed to design a torque controller using the kinematic control law developed in Section 3.1. Hence, the auxiliary backstepping error signal is defined by:

$$\boldsymbol{\eta} = \mathbf{u}_{\mathrm{k}} - \mathbf{u}, \tag{42}$$

where $\mathbf{u}_{\mathrm{k}}$ denotes the kinematic control law (34) and $\mathbf{u}$ denotes the transformed input vector defined in (21). Hence, the dynamic equations (23) can be reformulated as:

$$[\overline{\mathbf{M}}\dot{\mathbf{u}}_{\mathrm{k}} + \overline{\mathbf{V}}_{\mathrm{m}}\mathbf{u}_{\mathrm{k}} + \overline{\mathbf{N}}] + \bar{\boldsymbol{\tau}}_{\delta} - \overline{\mathbf{M}}\dot{\boldsymbol{\eta}} - \overline{\mathbf{V}}_{\mathrm{m}}\boldsymbol{\eta} = \overline{\mathbf{B}}\boldsymbol{\tau}, \tag{43}$$

in which $\|\bar{\boldsymbol{\tau}}_{\delta}\| \leqslant \tau_0$. Corresponding to Property 3, the bracket term can be linearly parameterized as:

$$\overline{\mathbf{M}}\dot{\mathbf{u}}_{\mathrm{k}} + \overline{\mathbf{V}}_{\mathrm{m}}\mathbf{u}_{\mathrm{k}} + \overline{\mathbf{N}} = \boldsymbol{\Upsilon}\vartheta. \tag{44}$$

Suppose that the system parameters are upper bounded as:

$$\|\vartheta\| \leqslant \vartheta_{\mathrm{M}}, \tag{45}$$

where ϑ_{M} is a known positive constant. It should be noted that this assumption is not restrictive and is always held in practical applications. The dynamic term $\boldsymbol{\kappa}$ is defined as:

$$\boldsymbol{\kappa} = \overline{\mathbf{M}}\dot{\mathbf{u}}_{\mathrm{k}} + \overline{\mathbf{V}}_{\mathrm{m}}\mathbf{u}_{\mathrm{k}} + \overline{\mathbf{N}} + \bar{\boldsymbol{\tau}}_{\delta} = \boldsymbol{\Upsilon}\vartheta + \bar{\boldsymbol{\tau}}_{\delta}. \tag{46}$$

Consequently, the error dynamic can be expressed as:

$$\overline{\mathbf{M}}\dot{\boldsymbol{\eta}} = -\overline{\mathbf{V}}_{\mathrm{m}}\boldsymbol{\eta} + \boldsymbol{\kappa} - \overline{\mathbf{B}}\boldsymbol{\tau}. \tag{47}$$

Proposition 2. *The torque control law given in* (34) *and* (35) *and:*

$$\boldsymbol{\tau} = (\overline{\mathbf{B}})^{-1}[\hat{\boldsymbol{\kappa}} - \mathbf{z}^* + z_3\mathbf{J}(\mathbf{z}^* + 2\mathbf{x}_{\mathrm{d}}^*) + k_{\eta}\boldsymbol{\eta} + \mathbf{h}_{\eta}], \tag{48}$$

and adaptation law:

$$\dot{\hat{\vartheta}} = \mathbf{\Gamma}\mathbf{\Upsilon}^{\mathrm{T}}\boldsymbol{\eta} - k_{\vartheta}\|\mathbf{Z}\|\mathbf{\Gamma}\hat{\vartheta}, \tag{49}$$

ensures GUUB tracking and regulation of (23)*, where* $\mathbf{h}_{\eta} = \frac{\tau_0^2}{\tau_0\|\boldsymbol{\eta}\|+\varepsilon_{\eta}}\boldsymbol{\eta}$*,* $\hat{\boldsymbol{\kappa}} = \mathbf{\Upsilon}\hat{\vartheta}$ *is the best estimation of dynamic term* $\boldsymbol{\kappa}$*,* $\mathbf{\Gamma} \in \Re^{p\times p}$ *is the adaptation gain matrix, and* k_{η}, k_{ϑ} *and* ε_{η} *are positive control gains.*

Proof. The positive control gains k_1', k_2' and k_{η}' are defined as:

$$k_i' = k_i - k_s, \quad i = 1, 2, \qquad k_{\eta}' = k_{\eta} - k_{\mathrm{s}}, \tag{50}$$

where k_{s} is a positive constant. In order to conclude on the stability of the system, the radially unbounded Lyapunov function:

$$V_2 = \frac{1}{2}\mathbf{z}^{*\mathrm{T}}\mathbf{z}^* + \frac{1}{2}z_3^2 + \frac{1}{2}\boldsymbol{\eta}^{\mathrm{T}}\overline{\mathbf{M}}\boldsymbol{\eta} + \frac{1}{2}\tilde{\vartheta}^{\mathrm{T}}\mathbf{\Gamma}^{-1}\tilde{\vartheta}, \tag{51}$$

is considered, where $\tilde{\vartheta} = \vartheta - \hat{\vartheta}$ is the parameter estimation error. According to Property 1, V_2 is a positive definite function. After taking the time derivative of (51), and using the torque control law (48), adaptation law (49) and invoking Property 2, the following equation is obtained:

$$\dot{V}_2 = -k_1\mathbf{z}^{*\mathrm{T}}\mathbf{z}^* - k_2 z_3^2 - k_{\eta}\boldsymbol{\eta}^{\mathrm{T}}\boldsymbol{\eta} + z_3(\rho - h_z) + \boldsymbol{\eta}^{\mathrm{T}}(\bar{\boldsymbol{\tau}}_{\delta} - \mathbf{h}_{\eta}) + k_{\vartheta}\|\mathbf{Z}\|\tilde{\vartheta}^{\mathrm{T}}\hat{\vartheta}. \tag{52}$$

According to Property 4, the following inequality can be simply derived:

$$\begin{aligned}\dot{V}_2 \leqslant{}& -k_1\|\mathbf{z}^*\|^2 - k_2 z_3^2 - k_{\eta}\|\boldsymbol{\eta}\|^2 + k_{\vartheta}\|\mathbf{Z}\|(\tilde{\vartheta}^{\mathrm{T}}\vartheta - \tilde{\vartheta}^{\mathrm{T}}\tilde{\vartheta}) \\ &+ \frac{\rho_0|z_3|}{\rho_0|z_3| + \varepsilon_z}\varepsilon_z + \frac{\tau_0\|\boldsymbol{\eta}\|}{\tau_0\|\boldsymbol{\eta}\| + \varepsilon_{\eta}}\varepsilon_{\eta}.\end{aligned} \tag{53}$$

Thus, using (50) yields:

$$\begin{aligned}\dot{V}_2 \leqslant{}& -k_{\mathrm{s}}\|\mathbf{Z}\|^2 - k_1'\|\mathbf{z}^*\|^2 - k_2' z_3^2 - k_{\eta}\|\eta\|^2 \\ &- k_{\vartheta}\|\mathbf{Z}\|\|\tilde{\vartheta}\|(\|\tilde{\vartheta}\| - \|\vartheta\|) + \varepsilon_z + \varepsilon_{\eta} \\ \leqslant{}& -k_{\mathrm{s}}\|\mathbf{Z}\|^2 - [k_{\min}'\|\mathbf{Z}\|^2 + k_{\vartheta}\|\mathbf{Z}\|\|\tilde{\vartheta}\|(\|\tilde{\vartheta}\| - \vartheta_{\mathrm{M}}) - \varepsilon_0],\end{aligned} \tag{54}$$

where $k_{\min}' = \min\{k_1', k_2', k_{\eta}'\}$, $\varepsilon_0 = \varepsilon_{\mathrm{z}} + \varepsilon_{\eta}$ and $\mathbf{Z}(t) = [\mathbf{z}^{\mathrm{T}}(t) \;\; \boldsymbol{\eta}^{\mathrm{T}}(t)]^{\mathrm{T}}$ is the augmented state vector. It can be easily proved that if $k_{\vartheta} = \frac{6\sqrt{k_{\min}'\varepsilon_0}}{\vartheta_{\mathrm{M}}^2}$ then the bracket term will be always nonnegative, provided that:

$$\|\mathbf{Z}\| \geqslant 2\sqrt{\frac{\varepsilon_0}{k_{\min}'}} = \sigma. \tag{55}$$

Therefore, $\dot{V}_2$ is negative outside a compact set, and due to the fact that V_2 is positive definite and radially unbounded, according to the standard Lyapunov theory extension, this demonstrates the GUUB stability of both $\|\mathbf{Z}\|$ and $\|\tilde{\vartheta}\|$ [29, 30]. QED.

Remark 4. Based on (51), (54) and (55), it can be concluded that $V_2(t) \in \ell_\infty$. Thus $\mathbf{z}(t), \boldsymbol{\eta}(t), \tilde{\vartheta}(t) \in \ell_\infty$. Using (29) and observing the fact that $\boldsymbol{\Psi}(t), \boldsymbol{\xi}(t) \in \ell_\infty$, it can be concluded that $\mathbf{x}_\mathrm{d}^*(t) \in \ell_\infty$. Thus, (28) can be employed to conclude that $\mathbf{x}(t) \in \ell_\infty$. Based on (30), it is obvious that $\dot{\boldsymbol{\Psi}}(t) \in \ell_\infty$. Utilizing (35) concluded that $u_\mathrm{w}(t) \in \ell_\infty$. Thus, $\dot{\mathbf{x}}_\mathrm{d}^* \in \ell_\infty$ and, therefore, from (34) it can be concluded that $\mathbf{u}_\mathrm{k}(t) \in \ell_\infty$. Then, from (42) $\mathbf{u}(t) \in \ell_\infty$. According to (33), $\dot{\mathbf{z}}(t) \in \ell_\infty$. Therefore, $\dot{\mathbf{h}}_z(t) \in \ell_\infty$ and noting that $\ddot{\boldsymbol{\Psi}}(t), \dot{\boldsymbol{\xi}}(t) \in \ell_\infty$, it can be concluded that $\dot{u}_w(t) \in \ell_\infty$, and, thus, from (34) $\dot{\mathbf{u}}_\mathrm{k}(t) \in \ell_\infty$. From (46) $\boldsymbol{\kappa} \in \ell_\infty$ and consequently $\boldsymbol{\Upsilon} \in \ell_\infty$. Thus, based on the definition of $\tilde{\vartheta}$ we have $\hat{\vartheta} \in \ell_\infty$ and then $\hat{\boldsymbol{\kappa}} \in \ell_\infty$. Finally, from (12) and (24), matrix $\overline{\mathbf{B}}$ is invertible and, thus, exploiting (48) it is concluded that $\boldsymbol{\tau} \in \ell_\infty$.

Remark 5. It has been noted that the first term of (49) is the standard adaptation law. The second term corresponds to the e-modification [30] from the adaptive control theory to guarantee the boundedness of parameter estimates.

3.3. Supervisory Fuzzy Control

The second equation of (11) expresses the lateral motion dynamics known as internal dynamics due to the fact that the lateral velocity cannot be controlled by $\boldsymbol{\tau}$. Thus, it is important to investigate the stability of internal dynamics during the robot motion. Also consider the case that all of the robot wheels skid laterally in the same direction, which practically causes the loss of motion stability. Hence, in order to move the robot properly, we propose a higher-level fuzzy controller as a supervisory control based on the following conditions:

- The internal dynamics is stable.
- The x-axis projection of ICR is held on the robot wheelbase, i.e., $-b < x_\mathrm{icr} < a$.

It has been emphasized that the supervisory fuzzy controller has been utilized to derive gains of the robust adaptive controller in a manner that the above condition holds during the robot motion. First, consider the Lyapunov function $V_3 = \frac{1}{2}v_y^2$. It is obvious that if $v_y \dot{v}_y \leqslant 0$, then the lateral motion dynamics is stable in the sense of Lyapunov stability. Also, the x-axis projection of ICR can be expressed as:

$$x_\mathrm{icr} = -\frac{v_y}{\Omega}. \tag{56}$$

Therefore, if $c|\Omega| - |v_y| > 0$ where $c = \min\{a, b\}$, then $-b < x_\mathrm{icr} < a$.

Figure 3 shows a fuzzy logic controller in which inputs are $-v_y[\frac{1}{m}(F_\mathrm{yf} + F_\mathrm{yb}) - v_x\Omega]$ and $c|\Omega| - |v_y|$, and output is K, which is used for control gains k_1, k_2 and k_η.

Based on the above discussion, if the inputs are positive, the lateral motion stability will be satisfied. The input and output membership functions are shown in Fig. 4 and the rule base is addressed in Table 1.

Membership functions of the fuzzy controller were obtained by trial and error, and supposed to be simple triangular and trapezoidal ones. In this case, it is not

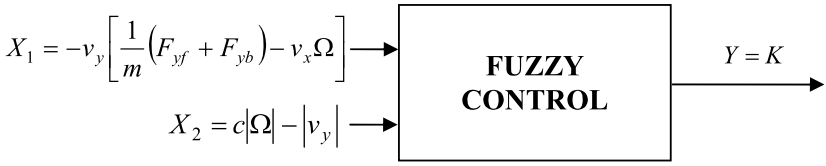

Figure 3. Fuzzy logic controller.

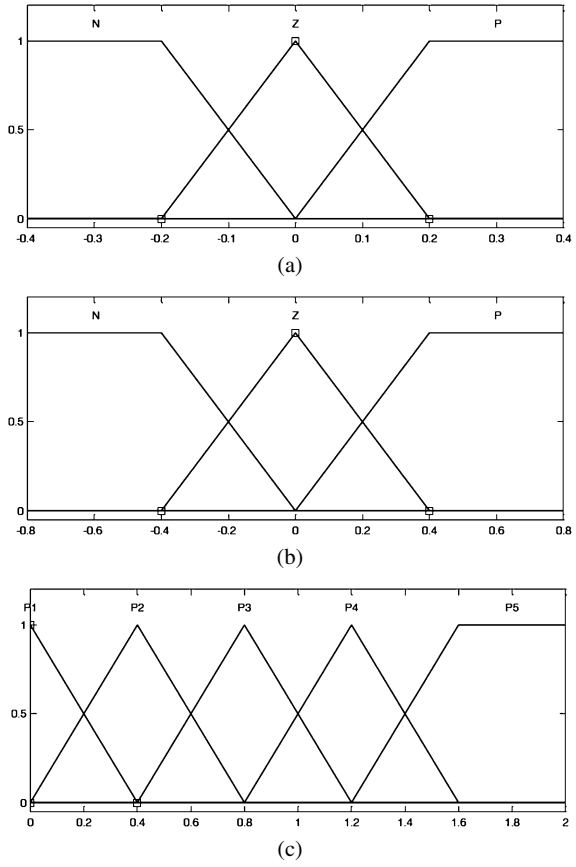

Figure 4. Input and output membership functions. (a) X_1, (b) X_2 and (c) Y.

necessary to design a complicated self-organized fuzzy control that increases the run time of the controller, while a simple knowledge-based one can provide our requirements. The logic to design the rule base of fuzzy controller is maintaining the lateral motion stability. In other words, whenever the input is large enough, the control gains will be large to increase the convergence speed and when the input is going to be small, the control gains will be small to prevent the lateral skidding of the robot. For example, rule 1 means that if inputs are P, then output is P5. In other words, the gains of the robust adaptive controller are assumed to be the largest to

increase convergences speed if $-v_y\dot{v}_y$ and $c|\Omega| - |v_y|$ are taken as relatively big positive amounts.

4. Simulation Results

In order to validate analytical developments, the robust adaptive stabilizing controller is implemented on a SSWMR using ADAMS. The P3AT skid steer mobile robot manufactured by ActivMedia Robotics is modeled using the graphical user interface of ADAMS View. The various components of the robot are generated with the robot parameters given in Table 2 and these are assembled together in a main assembly as shown in Fig. 5. It has been assumed that suspension of the robot is neglected and the robot moves on a horizontal surface. SI units and the SAE coordinate system have been used while modeling the robot, with x forward, y to the right and z downward. The Pacejka's magic formula tire model was utilized for modeling of the tire forces and flat road profile '2d_flat.rdf', available in the ADAMS

Table 1.
Rule base of fuzzy controller

Rule	X_1	X_2	Y
1	P	P	P5
2	P	Z	P4
3	P	N	P3
4	Z	P	P4
5	Z	Z	P3
6	Z	N	P2
7	N	P	P3
8	N	Z	P2
9	N	N	P1

Table 2.
Robot parameters

Parameter	Value
m	40.4 kg
I_z	0.512 kgm^2
I_w	0.01 kgm^2
n	49.8
a	0.138 m
b	0.122 m
r	0.1075 m
t	0.1975 m

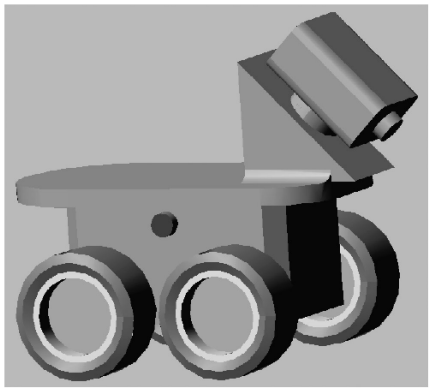

Figure 5. ADAMS modeling of P3AT.

Table 3.
Robust adaptive controller parameters

Parameter	Value
k_s	0.1
$a_1 = a_2$	2
$\alpha_1 = \alpha_2$	0.25
ρ_0	0.4
$\varepsilon_1 = \varepsilon_2 = \varepsilon_z = \varepsilon_\eta$	0.02
$\mathbf{\Gamma}$ for Case A	diag{0.12, 0.002, 100, 100}
$\mathbf{\Gamma}$ for Case B	diag{0.12, 0.002, 100}

database, is used for road modeling. The model created by ADAMS has been used as the system plant in simulations.

The initial posture is assumed to be $\mathbf{q}(0) = [0 \;\; 1 \;\; 0]^{\mathrm{T}}$. To investigate the wheel's slippage effects, simulations are performed for the two cases discussed in Section 2.1: Case A, when wheel dynamics and tire slippage are considered, and Case B, without wheel dynamics and tire slippage effects. For more effective comparison, simulations are performed for two different tire–ground friction coefficients. In simulation 1 we assume that $\mu = 0.5$ and simulation 2 $\mu = 0.3$.

The robust adaptive controller parameters are shown in Table 3. Also, note that $k_1 = k_2 = k_\eta = K$, where K is the fuzzy control output.

The system parameters are given by vector $\vartheta = [m_e \;\; I_e \;\; m \;\; \mu m]^{\mathrm{T}}$ for Case A and $\vartheta = [m_e \;\; I_e \;\; \mu m]^{\mathrm{T}}$ for Case B. Assuming 30% error for the system parameters, simulation results are shown in Figs 6–8 for simulation 1 and Figs 9 and 10 for simulation 2.

4.1. Simulation 1: $\mu = 0.5$

Based on Figs 6a and b and 7a and b, the robust adaptive controller can stabilize the robot posture to a small neighborhood of the final posture. Considering Figs 6c and

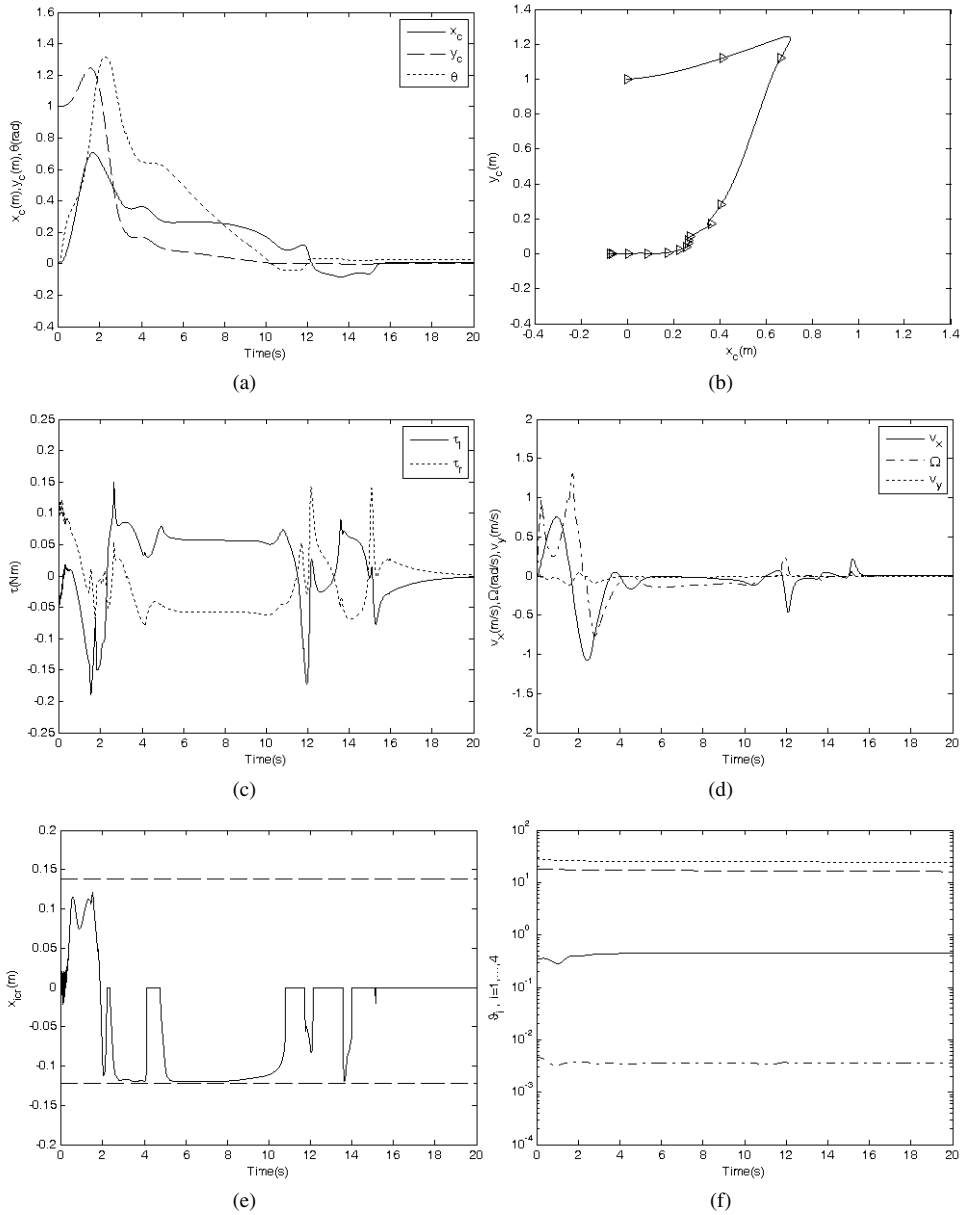

Figure 6. Simulation results for Case A, $\mu = 0.5$. (a) Time response of the state variables. (b) Robot's path in task space. (c) Left and right control torques. (d) Longitudinal, lateral and angular velocities. (e) Longitudinal component of the ICR (limit values are depicted by the dashed line). (f) Estimated parameters.

7c, it can be observed that in the beginning of the robot's motion, the control torques in Case A are smaller than the corresponding ones in Case B. Also, oscillation of input torque in Case A is less than Case B. Based on Figs 6d and 7d, longitudinal

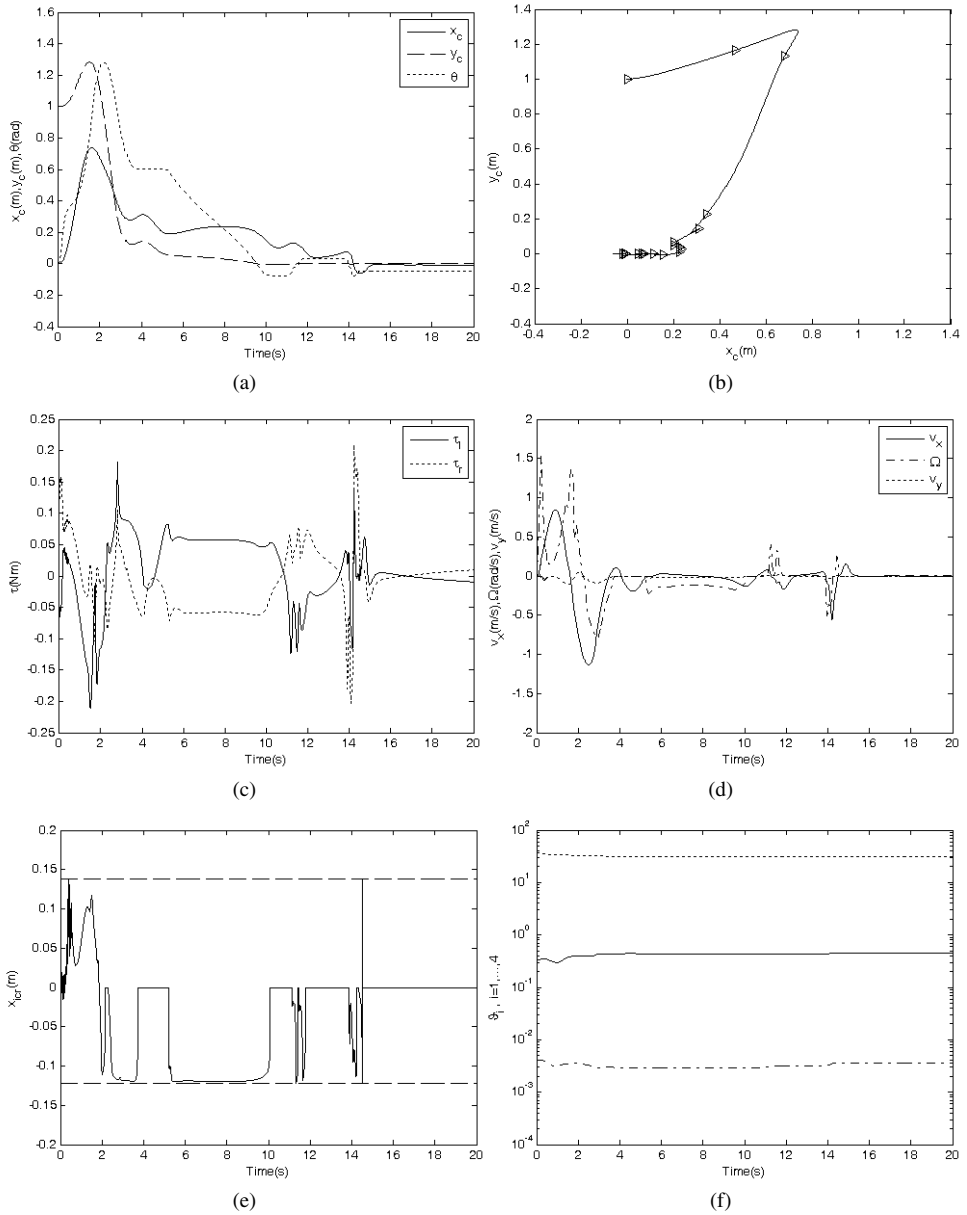

Figure 7. Simulation results for Case B, $\mu = 0.5$. (a) Time response of the state variables. (b) Robot's path in task space. (c) Left and right control torques. (d) Longitudinal, lateral and angular velocities. (e) Longitudinal component of the ICR (limit values are depicted by dash line). (f) Estimated parameters.

velocity of the robot's COM is smaller than 1.2 m/s (maximum velocity that P3AT can achieve). Also, for both cases the lateral velocity of the robot COM is less than 0.12 m/s and, thus, the inequality $|\rho| < \rho_0$, which is assumed in kinematic controller

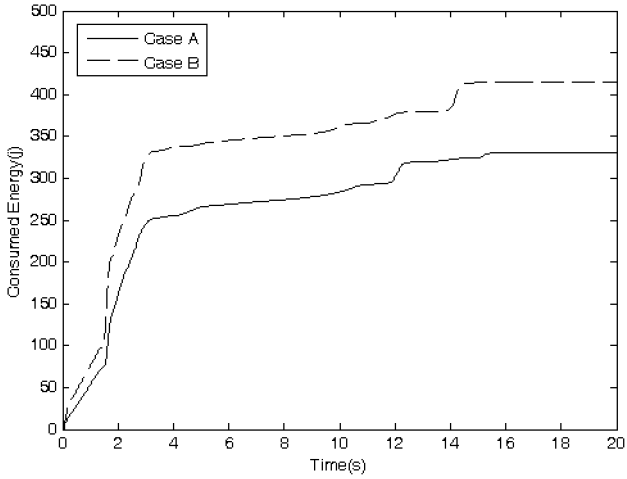

Figure 8. Total consumed energy for two cases, $\mu = 0.5$.

design (see (19)), is held during the robot motion. For both cases, the longitudinal component of the ICR is kept between bounds ($-a \leqslant x_{\text{icr}} \leqslant b$) as shown in Figs 6e and 7e. This implies the effectiveness of the supervisory controller. Finally, Figs 6f and 7f shows the estimated parameters that are bounded during the motion.

Note, that based on the Figs 6 and 7 in case of $\mu = 0.5$, there is a little difference between the two cases, and the robot motion is acceptable even for Case B, where the wheel dynamics and tire slippage are neglected and the lateral forces are simply derived by (16).

It has been noted that SSWMRs are energy consuming and thus energy is of prime importance for these kinds of robots [31]. Total consumed energy during the robot motion can be obtained by $\sum \tau_i \omega_i$. Based on Fig. 8, total consumed energy for Case A is 330.4 J and for Case B is 415.4 J. Therefore, when the effects of tire slippage and wheel dynamics are considered, 20% of energy was saved on these simulations. Therefore, although the robot motion is approximately similar in the two cases, the total consumed energy is not.

4.2. Simulation 2: $\mu = 0.3$

Here, some plots have been not shown for brevity's sake. Based on Figs 9a and b and 10a and b, although the robust adaptive controller can stabilize the robot posture to a small neighborhood of the final posture, in Case B robot motion is more oscillatory than Case A. Considering Figs 9c and 10c it can be observed that the control torques in Case A are significantly smaller than the corresponding ones in Case B. Also, oscillation of input torque in Case A is considerably less than Case B. It has been noted for the two cases that control torques are larger than the corresponding ones in simulation 1. In fact, when the robot moves on a relatively slippery surface, wheel slippage increases and then tire forces, as a function of slip ratio and slip angle, will be increased too.

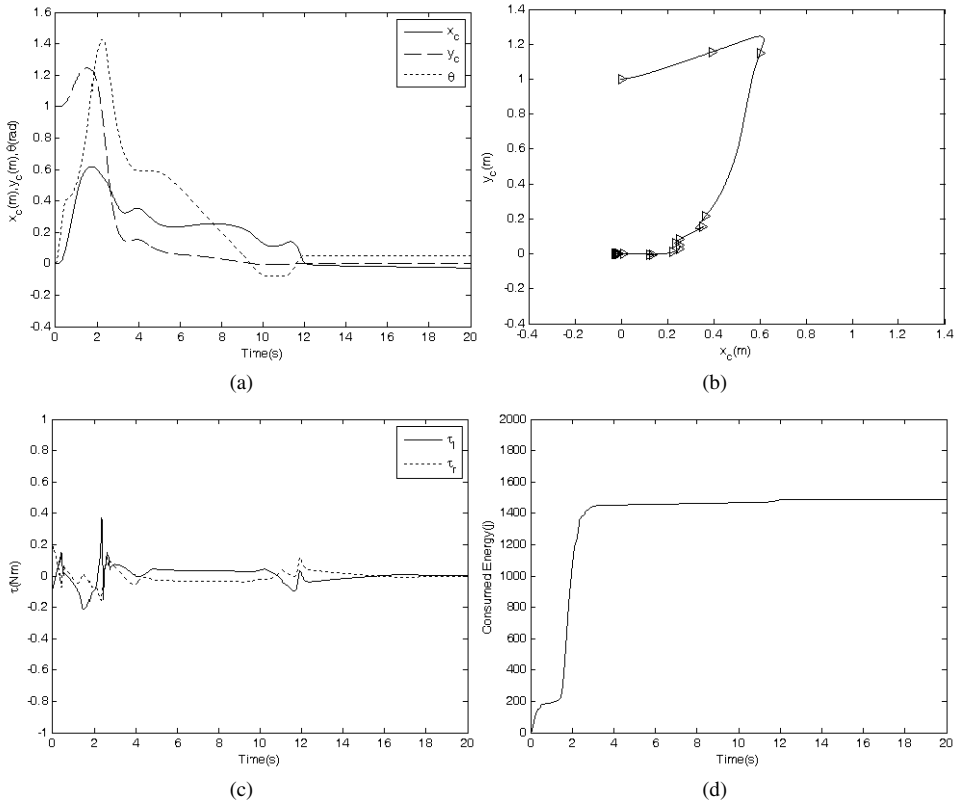

Figure 9. Simulation results for Case A, $\mu = 0.3$. (a) Time response of the state variables. (b) Robot's path in task space. (c) Left and right control torques. (d) Total consumed energy.

In addition, based on Figs 9d and 10d, total energy consumed for Case A is 1488 J, which is considerably lees than the corresponding one for Case B, i.e., 10715 J. Therefore, when robot moves on a relatively slippery surface, a large amount of energy would be saved if the effects of tire slippage and wheel dynamics were considered. It has been noted that for the two cases the total consumed energy is larger than the corresponding values in simulation 1. In fact, when robot moves on a relatively slippery surface, robot wheel velocities increase, leading to enlargement of the total consumed energy.

5. Conclusion

In this paper, dynamic robust adaptive stabilizing control of a Skid SSWMR was studied. The effects of longitudinal slipping and wheel dynamics were considered, and GUUB stability of the system to an arbitrarily small neighborhood of the origin was proved. A supervisory fuzzy logic-based controller was designed to keep the ICR within robot wheelbase during the motion and the stability of internal dynamics was established. Simulation results favorably support the analytical developments

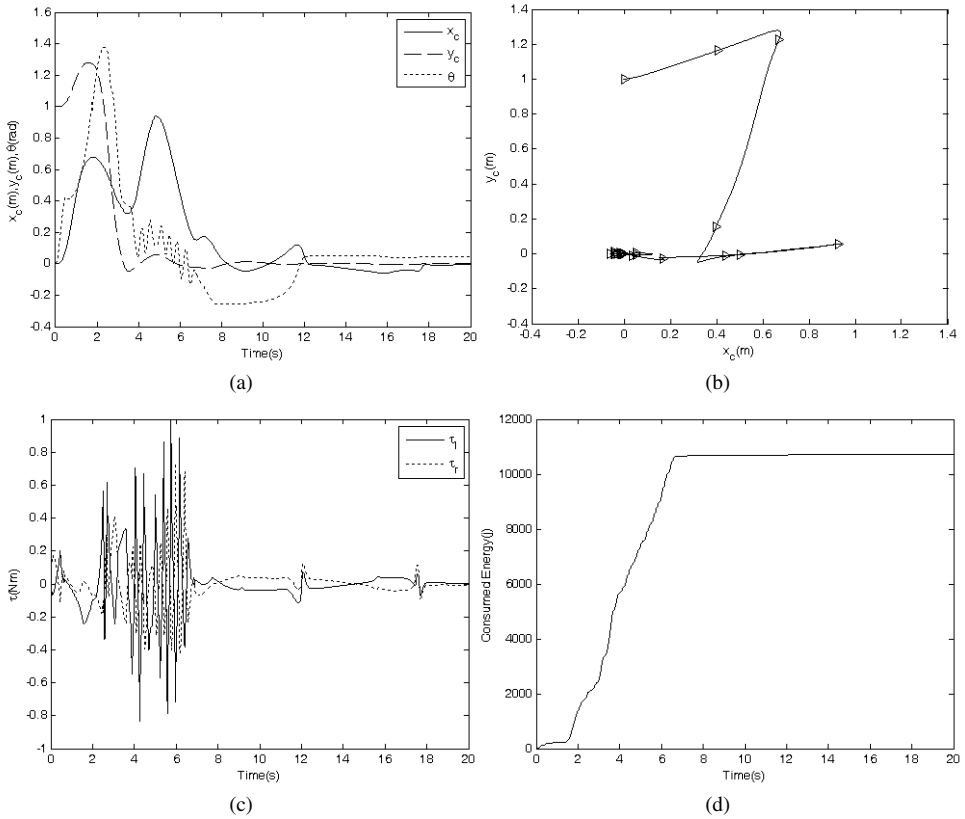

Figure 10. Simulation results for Case B, $\mu = 0.3$. (a) Time response of the state variables. (b) Robot's path in task space. (c) Left and right control torques. (d) Total consumed energy.

and effectiveness of the proposed controller. Based on the simulations, when a robot moves on a relatively rough ground surface, robot, motion was acceptable even for the case that the wheel dynamics and tire slippage were neglected and the lateral forces are highly simplified by Coulomb friction. However, when a robot moves on a relatively slippery surface, the effect of wheel dynamics and tire slippage have to be taken into account to prevent oscillatory behavior of the robot and reduce the total consumed energy. Future works are dedicated to the implementation of the proposed controllers on a real mobile robot.

References

1. W. Leroquais and B. d'Andrea-Novel, Modeling and control of wheeled mobile robots not satisfying ideal velocity constraints: the unicycle case, in: *Proc. Conf. on Decision and Control*, Kobe, pp. 1437–1442 (1996).
2. I. Motte and G. Campion, A slow manifold approach for the control of mobile robots not satisfying the kinematic constraints, *IEEE Trans. Robotics Automat.* **16**, 875–880 (2000).
3. T. Urakubo, K. Tsuchiya and K. Tsujita, Motion control of a two-wheeled mobile robot, *Adv. Robotics* **15**, 711–728 (2001).

4. Y. Zhang, J. H. Chung and S. A. Velinsky, Variable structure control of a differentially steered wheeled mobile robot, *J. Intell. and Robotic Syst.* **36**, 301–314 (2003).
5. Z. P. Wang, C. Y. Su, T. H. Lee and S. S. Ge, Robust adaptive control of a wheeled mobile robot violating the pure nonholonomic constraint, in: *Proc. Int. Conf. on Control, Automation, Robotics and Vision*, Kumming, pp. 987–992 (2004).
6. C. B. Low and D. Wang, GPS-based tracking control for a car-like wheeled mobile robot with skidding and slipping, *IEEE/ASME Trans. Mechatron.* **13**, 480–484 (2008).
7. C. B. Low and D. Wang, GPS-based path following control for a car-like wheeled mobile robot with skidding and slipping, *IEEE Trans. Control Syst. Technol.* **16**, 340–347 (2008).
8. D. Wang and C. B. Low, Modeling and analysis of skidding and slipping in wheeled mobile robots: control design perspective, *IEEE Trans. Robotics* **24**, 676–687 (2008).
9. F. N. Martins, W. C. Celeste, R. Carelli, M. Sarcinelli-Filho and T. F. Bastos-Filho, An adaptive dynamic controller for autonomous mobile robot trajectory tracking, *Control Eng. Pract.* **16**, 1354–1363 (2008).
10. J. Ploeg, H. E. Schouten and H. Nijmeijer, Control design for a mobile robot including tire behavior, in: *Proc. IEEE Intelligent Vehicles Symp.*, Eindhoven, pp. 240–245 (2008).
11. L. Caracciolo, A. D. Luca and S. Iannitti, Trajectory tracking control of a four wheeled differentially driven mobile robot, in: *Proc. IEEE Conf. on Robotics and Automation*, Detroit, MI, pp. 2632–2638 (1999).
12. E. Maaloufa, M. Saada and H. Saliahb, A higher level path tracking controller for a four-wheel differentially steered mobile robot, *Robotics Autonomous Systems* **54**, 23–33 (2006).
13. J. Yi, D. Song, J. Zhang and Z. Goodwin, Adaptive trajectory tracking control of skid-steered mobile robots, in: *Proc. IEEE Int. Conf. on Robotics and Automation*, Rome, pp. 2605–2610 (2007).
14. R. W. Brockett, Asymptotic stability and feedback stabilization, in: *Differential Geometric Control Theory*, pp. 181–191. Birkhauser, Boston, MA (1983).
15. A. M. Bloch, M. Reyhanoglu and N. H. McClamroch, Control and stabilization of nonholonomic dynamic systems, *IEEE Trans. Automatic Control* **37**, 1746–1757 (1992).
16. C. Samson, Control of chained systems application to path following and time-varying point-stabilization of mobile robots, *IEEE Trans. Automatic Control* **40**, 64–77 (1995).
17. C. Canudas de Wit and O. J. Sørdalen, Exponential stabilization of mobile robots with nonholonomic constraints, *IEEE Trans. Automatic Control* **37**, 1791–1797 (1992).
18. S. S. Ge, J. Wang, T. H. Lee and G. Y. Zhou, Adaptive robust stabilization of dynamic nonholonomic chained systems, *J. Robotic Syst.* **18**, 119–133 (2000).
19. W. E. Dixon, M. S. de Queiroz, D. M. Dawson and T. J. Flynn, Adaptive tracking and regulation of a wheeled mobile robot with controller/update law modularity, *IEEE Trans. Control Syst. Technol.* **12**, 138–147 (2004).
20. B. L. Ma and S. K. Tso, Robust discontinuous exponential regulation of dynamic nonholonomic wheeled mobile robots with parameter uncertainties, *Int. J. Robust Nonlinear Control* **18**, 960–974 (2007).
21. M. L. Corradini, T. Leo and G. Orlando, Robust stabilization of mobile robot violating the nonholonomic constraint *via* quasi-sliding modes, in: *Proc. American Control Conf.*, San Diego, CA pp. 3935–3939 (1999).
22. W. E. Dixon, D. M. Dawson and E. Zergeroglu, Robust control of a mobile robot system with kinematic disturbances, in: *Proc. IEEE Int. Conf. on Control Applications*, pp. 437–442 (2000).
23. K. Kozlowski and D. Pazderski, Modeling and control of a 4-wheel skid-steering mobile robot, *Int. J. Appl. Math. Comput. Sci.* **14**, 477–496 (2004).

24. W. E. Dixon, D. M. Dawson, E. Zergeroglu and A. Behal, *Nonlinear Control of Wheeled Mobile Robots*. Springer, Berlin (2001).
25. K. Kozlowski and D. Pazderski, Practical stabilization of a skid-steering mobile robot — a kinematic-based approach, in: *Proc. IEEE 3rd Int. Conf. on Mechatronics*, Budapest, pp. 519–524 (2006).
26. D. Pazderski and K. Kozlowski, Trajectory Tracking of underactuated skid-steering robot, in: *Proc. Amer. Control Conf.*, Washington, DC, pp. 3506–3511 (2008).
27. R. Rajamani, *Vehicle Dynamics and Control*. Springer, New York (2006).
28. C. C. Ward and K. Iagnemma, A dynamic-model-based wheel slip detector for mobile robots on outdoor terrain, *IEEE Trans. Robotics*, **24**, 821–831 (2008).
29. F. Lewis, C. Abdallah and D. Dawson, *Control of Robot Manipulators*. Macmillan, London (1993).
30. K. S. Narendra and A. M. Annaswamy, A new adaptive law for robust adaptation without persistent excitation, *IEEE Trans. Automatic Control* **32**, 134–145 (1987).
31. B. Shamah, Experimental comparison of skid steering *vs.* explicit steering for a wheeled mobile robot, *MSc Thesis*, The Robotics Institute of Carnegie Mellon University (1999).
32. D. M. Dawson, J. Hu and T. C. Burg, *Nonlinear Control of Electric Machinery*. Dekker, New York, NY (1998).

Appendix

Lemma 1 [32]. *Supposing that $V(t)$ is a non-negative scalar function of time $t \geqslant 0$ that satisfies the differential inequality given by:*

$$\dot{V} \leqslant -\gamma V + \varepsilon, \tag{57}$$

where γ and ε are positive constants. Then, the following inequality holds:

$$\forall t \geqslant 0 \quad V(t) \leqslant V(0)\exp(-\gamma t) + \frac{\varepsilon}{\gamma}(1 - \exp(-\gamma t)). \tag{58}$$

About the Authors

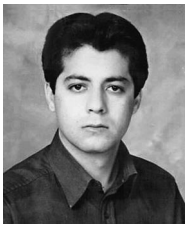

E. Mohammadpour received his BSc from the Department of Mechanical Engineering, Sharif University of Technology, Tehran, Iran, in 2002, and his MSc from the Department of Mechanical Engineering, AmirKabir University of Technology, Tehran, Iran, in 2004. He is currently a PhD student at the Mechanical Engineering, AmirKabir University of Technology. His research interests include dynamics and control of mobile robots and nonholonomic systems.

M. Naraghi received his BSc from the Department of Mechanical Engineering, University of Minnesota, Minneapolis, MN, USA, in 1981, his MS from the Department of Mechanical Engineering, Tarbiat Modarres University, Tehran, Iran, in 1989, and his PhD degree from the Department of Mechanical Engineering, University of Ottawa, Canada, in 1996. He has been with the Department of Mechanical Engineering at AmirKabir University of Technology since 1996. His research interests are in robotics and control, including both the theoretical and experimental studies.